Journal of Colloid and Interface Science **239,** 417–431 (2001)
doi:10.1006/jcis.2001.7594, available online at http://www.idealibrary.com on IDEAL®

The Effects of Void Geometry and Contact Angle on the Absorption of Liquids into Porous Calcium Carbonate Structures

Cathy J. Ridgway,* Joachim Schoelkopf,* G. Peter Matthews,†,[1] Patrick A. C. Gane,* and Philip W. James‡

*Omya AG, CH-4665 Oftringen, Switzerland; †Environmental and Fluid Modelling Group, Department of Environmental Sciences, University of Plymouth, Plymouth PL4 8AA, United Kingdom; and ‡Department of Mathematics and Statistics, University of Plymouth, PL4 8AA, United Kingdom

Received July 10, 2000; accepted March 28, 2001

The absorption (permeation) of alcohols into porous blocks of calcium carbonate has been studied experimentally and with a computer model. The experimental measurement was of change in apparent weight of a block with time after contact with liquid. The modeling used the previously developed 'Pore-Cor' model, based on unit cells of 1000 cubic pores connected by cylindrical throats. To gain some insight into absorption into voids of complex geometry, and to provide a representation of heterogeneities in surface interaction energy, the cylindrical throats were converted to double cones. Relative to cylinders, such geometries caused hold-ups of the percolation of nonwetting fluids with respect to increasing applied pressure, and a change in the rate of absorption of wetting fluids. Both the measured absorption of the alcohols and the simulated absorption of the alcohols and of water showed significant deviations from that predicted by an effective hydraulic radius approximation. The simulation demonstrated the development of a highly heterogeneous wetting front, and of preferred wetting pathways that were perturbed by inertial retardation. The findings are useful in the design of high-performance, low-waste pigments for paper coatings, and environmentally friendly printing inks, as well as in wider industrial, environmental, and geological contexts.

Key Words: **coating pigment; environmentally friendly ink; imbibition; inertial flow; ink; liquid absorption; low-waste pigment; percolation; permeation; Pore-Cor; pore model; porosity; printing.**

INTRODUCTION

We present a study of the rate of permeation of alcohols into porous blocks of calcium carbonate. The investigation was carried out both experimentally and by means of a computer simulation. The computer simulation used previously developed software known as "Pore-Cor," and involved the incorporation of new, more complicated geometries within the simulated void structure. The motivation for the work was the interest being currently shown by the paper and printing industries in the design of high-performance paper coatings, using low-waste pigments, and in the use of environmentally friendly printing inks. Modern, high-speed printing techniques depend crucially on the absorption behavior of fluids into paper coatings at times that are too short to measure in the laboratory. There is also a wider interest in fluid absorption, since it is an important feature of a variety of other industrial, technological, and environmental processes, as diverse as the operation of fuel cells, the movement of oil in reservoir sandstone, and the migration of pollutants in soil. This work has provided additional functionality to the Pore-Cor software, which is being used by other workers in such fields.

There are two features of this new application of the computer model that are worthwhile to discuss at the outset, since they provide both benefits and drawbacks. The first is the incorporation of more complex void geometries, specifically double-conical throats. Previously, the Pore-Cor computer model of void structure has comprised a unit cell of 1000 cubic pores connected by up to 3000 cylindrical throats in each Cartesian direction. Converting the cylinders to double cones introduces a new degree of complexity to the structure. The arbitrary nature of this additional geometrical complexity must be compensated by the additional insights that the complexity brings to the study. New insights were indeed gained, but for reasons explained below, the additional arbitrariness is only partially dealt with. The second feature is that of the time interval. Because of the mathematical complexity of the new calculation, the computer model could only be stepped forward at intervals of 1 ns, and run up to times of around 0.1 s after contact between the solid and liquid. Fortunately, these intervals span the times of interest in high-speed printing processes. However, they are very difficult to access experimentally, both in terms of instrumentation, and because when the solid and fluid contact each other, there is an interval of a substantial fraction of a second during which the meniscus jumps from the liquid surface to join it to the solid, followed by a few seconds of oscillation (1). Therefore, the experiments covered the time period of 0.4 s to 22 h after contact, and experiment and simulation could only be compared by extrapolation of the results toward each other in the time domain.

The rate of fluid permeation is initially dependent on the sizes and shapes of the voids at, or close to, the surface of the sample that is in contact with the fluid. The subsequent rate of permeation depends on the sizes and geometries of the neighboring

[1]To whom correspondence should be addressed.

0021-9797/01 $35.00

voids. The subsequent rate also depends on the way in which these neighboring voids are connected to the surface voids and to each other to form a three-dimensional void network. When the fluid is nonwetting, the permeation is also referred to as intrusion or percolation, and when wetting, as imbibition or absorption. The latter terminology has been commonly used in past studies by other workers, and we therefore adopt it in this work. Many past studies have focused on the exact geometry of the voids within a wide range of samples. However, to model the absorption of fluid into a large array of voids within a porous sample, it is necessary to make major simplifying approximations. As stated above, these have previously involved the assumption of cylindrical throats. However, the unrealistic nature of such an approximation can be readily demonstrated by, for example, the microscopy of a Woods metal cast of void structure (2), or the image analysis of tomographs of nuclear magnetic resonance signals (3). Computational constraints dictate that the cylindrical throat geometry must be replaced by another arbitrary but realistic geometry rather than by truly random shapes. We have chosen divergent–convergent double cones, since these generate concave cavities similar to those often found in natural samples, present different surface angles to the permeating fluid, and have calculable absorption properties. We describe the effect of these throat geometries on the percolation of a nonwetting fluid (mercury), and on the rate of absorption of several wetting fluids. Rather than using an arbitrary network containing these double-conical throats, we generate a network that has the same percolation characteristics to mercury as found in a porous block of compressed particulate calcium carbonate. The calcium carbonate is of a type used as a major component of some high-performance paper coatings in the printing industry. The rates of absorption of a range of wetting fluids into the simulated network are compared with experimental measurements of absorption into the calcium carbonate samples. The simulated and experimental rates are found to agree both in the overall rate profiles, and in the trend with different liquids. The work builds on, and incorporates, a previous study, in which we demonstrated the effect of fluid momentum on the initial absorption of wetting liquids into our Pore-Cor network model with cylindrical throats (1).

The case of a nonwetting fluid passing from a cylindrical throat into a spherical pore, or into a pore with a sinusoidal entry, has been calculated by Tsakiroglou and Payatakes (4). With regard to other geometries, Borhan and Rungta (5) have investigated the wetting of periodically corrugated plates, and there have been many studies of menisci in other noncylindrical tubes (6–11). Maisch *et al.* (12) have investigated the effect of geometric discontinuities along the axial direction of a tube.

The local variations in a natural sample may be caused by the fluid passing over a different crystal plane (13), or because the void structure contains inclusions such as illite and smectite clay (14). The determination of discrete local free energies is not normally possible, and so studies tend to measure average interaction energies (15). In this study, local heterogeneities in surface energies are not explicitly modeled, but are reflected in the local variations in capillary pressure and absorption speed caused by the double-conical throats.

Previous experimental studies of absorption have been briefly reviewed in a previous publication (1). In most of these studies, the absorption of a fluid into a porous void network was approximated as the absorption of a fluid into a single tube, or a bundle of parallel tubes that are all of the same radius R. We refer to this as the effective hydraulic radius (EHR) approximation.

The Pore-Cor Network Model

Pore-Cor is a computer model that simulates the void-space structure of porous materials. It has been used to simulate the structures of a wide range of porous materials including sandstones (14), medicinal tablets (16), and soil (17). Pore-Cor uses a unit cell with 1000 cubic pores in a $10 \times 10 \times 10$ array, connected by up to 3000 throats (i.e., one connected to each cube face). Each pore is equally spaced from its neighboring pores by the "pore row spacing" Q, and each unit cell is a cube of side length $10Q$. There are periodic boundary conditions: i.e., each unit cell is connected to another identical unit cell in each direction. The pore-size and throat-size distributions of the unit cell are optimized so that the simulated percolation curve fits as closely as possible to the corrected experimental mercury intrusion curve (18). The pore- and throat-size distributions are characterized by two parameters, "throat skew" and "pore skew." The distribution of throat sizes is log–linear. The throat skew is the percentage number of throats of the smallest size. The log–linear distribution pivots about its midpoint (geometric mean) at 1%, so that if there are 1.15% of the smallest throat sizes, there will be 0.85% of the largest throat sizes. The pore skew increases the sizes of the pores by a constant multiple, for example, 1.4. However, the pores with the largest sizes are truncated back to the size of the largest throat, thus giving a peak in the number of pores with this largest permitted size. The positions of the pores and throats are random, determined by a pseudo-random number generator. The percolation characteristics of the network are insensitive to Q. Therefore, after convergence of the simulated percolation to the experimental percolation has been achieved by scanning through values of throat skew and connectivity (the average number of throats connecting to a pore), Q is adjusted so that the porosity matches the experimental value while ensuring that no pores overlap. The parameters and procedure are described in more detail in previous publications (16, 18).

It is not normally possible to represent the complexity of the void network of a natural sample using the relatively simple geometry of the Pore-Cor unit cell. Also, the size of the unit cell is often smaller than the representative elementary volume (REV) of the sample. Therefore, different unit cells must be generated using a different seed for the pseudo-random number generator. The model is designed so that different structural parameters in conjunction with the same seed of the pseudo-random number generator produce a family of unit cells that are similar to each other—for example, all may have a group of large pores in the same region. Each family is referred to as a stochastic generation.

This aspect of the modeling is discussed in detail in a recent publication (17).

THEORY

Permeation of a Fluid into Cylindrical Throats

Many simulations of void networks, including the previous version of Pore-Cor, assume cylindrical throats. The percolation of a nonwetting fluid such as mercury into one of these throats is then calculated by the Laplace equation

$$P = \frac{2\gamma \cos\theta}{r}, \qquad [1]$$

where P is the applied pressure of the nonwetting fluid, γ is its surface tension, θ is the contact angle between the fluid and the wall of the throat, and r is the throat radius. The equation does not include time as a parameter, and therefore neither does the simulated percolation. Instead, the percolation is represented as an extent of penetration for any particular applied pressure P, where P is assumed constant throughout the mass of fluid. If the applied pressure exceeds that required for the fluid to intrude a particular feature within the array, and the geometry of the array is such that fluid has reached the feature, then fluid will intrude. If there are larger, empty features connected to the newly filled feature, then they will be intruded also. If the applied pressure is increased further, more features will be intruded until the whole network is full. At each applied pressure, the system is "quasi-static"—i.e., each feature will be either completely empty or completely full of fluid. There is no explicit measure of the rate of intrusion into any feature nor, correspondingly, of the nature of the flow. In the literature, such flow is referred to as "piston-like"—a description that is imprecise but nevertheless sufficiently useful to be used in this work.

Washburn (19) and Lucas (20) obtained a time-dependency for the uptake of a wetting fluid into a cylinder, by assuming that the flow was laminar and could therefore be described by both the Poiseuille and Laplace equations. Their expression is

$$x^2 = \frac{R\gamma t \cos\theta}{2\eta}, \qquad [2]$$

where x is the distance traveled by the liquid front in time t, R is the effective hydraulic radius, and η is the dynamic viscosity. Many permeation experiments show at least superficial agreement with [2], with an uptake distance approximately proportional to $\sqrt{t}$. The equation therefore continues to be used, despite the fact that in porous networks R, θ and γ have no precise physical basis. In this work, we use it to provide a baseline against which to measure our own measurements and simulations of fluid behavior.

Percolation of a Nonwetting Fluid into Conical Throats

As discussed previously, the void connections that correspond to the throats in natural samples are never perfectly cylindrical. Often the connections have a geometry that diverges from a narrow neck. Such divergence retards the intrusion of a nonwetting fluid, requiring an applied pressure above that required for a cylinder with the same entrance diameter to overcome the "hold-up." Such an effect can be simulated by changing the shape of the throats from cylinders to double cones. (The double cones are strictly double frustums because the cones are truncated.) Figure 1 shows this geometry in cross section. The fluid is initially contained in a cylinder of radius r. (In practice, in the Pore-Cor network, the double cones are joined directly onto the cubic pores, so these cylinders are of negligible length.) The position of the line of contact of the fluid with the wall of the cylinder or cone is characterized by the parameter x. Position 1 on the diagram is a typical position of the fluid in the cylinder—at this point the fluid would be moving in piston-like fashion toward the double cone. At position 2 ($x = 0$), the fluid begins to enter the diverging part of the double cone. The maximum radius of the double cone is $r_{\max}$. Its overall length is h and the length of the diverging cone is $h/2$ as shown. Therefore the angle at the entrance to the cone is $\omega = \tan^{-1}\{2(r_{\max} - r)/h\}$. We assume the contact angle of the intruding liquid, $\theta_I = \pi - \theta$, remains constant whatever the angle of the surface. Therefore, as the meniscus enters the diverging cone, position 2, the meniscus bulges as shown. Although the contact angle θ_I is the same, the force acting along the contact line between the meniscus and the solid surface is now at an angle β to the axial direction, where $\beta = \omega - \theta_I$. As the fluid moves to position 3, the feature radius r_{cone} increases as $(r + x\tan\omega)$. The hold-up pressure P_{holdup} is a function of r_{cone}, and is calculated by balancing the forces on

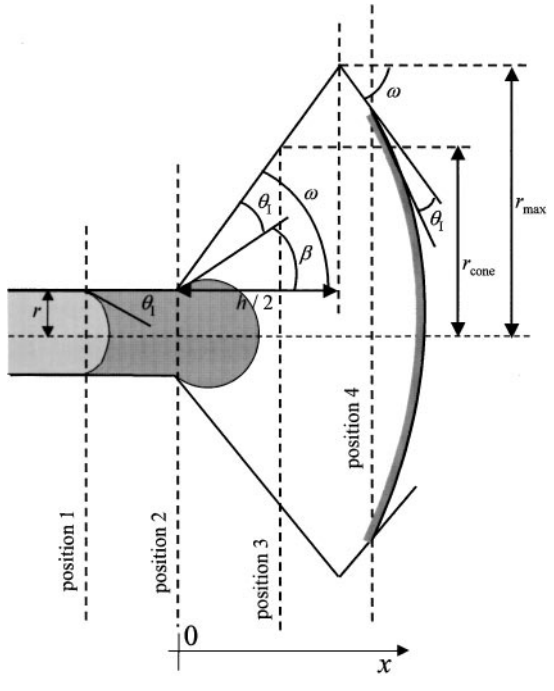

FIG. 1. Cross-sectional view of a nonwetting fluid entering a double-conical throat.

the fluid in the axial direction (4):

$$P_{\text{holdup}} = \frac{2\gamma \cos\beta}{r_{\text{cone}}} = \frac{2\gamma \cos\left[\tan^{-1}\left(\frac{2(r_{\max}-r)}{h}\right) - (\pi-\theta)\right]}{r_{\text{cone}}}. \quad [3]$$

As the intrusion of the fluid proceeds into the diverging part of the double cone, β remains constant but r_{cone} increases, so the hold-up pressure P_{holdup} decreases. Therefore, once the applied pressure has been increased sufficiently to overcome the initial hold-up, the intrusion continues spontaneously until the whole divergent cone is full ($x = h/2$).

When the meniscus enters the converging part of the cone, as represented by position 4, the meniscus is flattened relative to its shape at positions 1, 2, and 3. The component of the force is again proportional to $\cos\beta$, but β is now $(\omega + \theta_1)$ rather than $(\omega - \theta_1)$. The value of $\cos\beta$ will always be less for position 4 than for position 1, 2, or 3, and therefore intrusion of the convergent part for the double cone will also be spontaneous once the initial hold-up pressure is achieved. The intrusion of the double cone is, therefore, piston-like as for a cylinder. Consequently, in modeling the intrusion of a nonwetting fluid into a simulated network, it is often convenient to measure the intrusion in terms of the effective radius r_{eff} of a cylindrical throat with the same percolation characteristics:

$$r_{\text{eff}} = r\frac{\cos\theta_1}{\cos\beta} = \frac{-r\cos\theta}{\cos\left[\tan^{-1}\left(\frac{2(r_{\max}-r)}{h}\right) - (\pi-\theta)\right]}. \quad [4]$$

It is clear from the equation that if on average θ_1 for any particular feature is greater than β, then since both are angles between 0° and 90°, on average r_{eff} will be less than r. In this case, the pores within the structure will be more shielded by conical throats than by cylindrical throats of the same entry size. Thus it will take more pressure to intrude the structure with mercury, and the voids will appear smaller when investigated by porosimetry.

Absorption of a Wetting Fluid into Conical Throats

If a wetting fluid enters a double-conical throat, it will do so with a concave rather than convex meniscus, Fig. 2a. For the diverging part of the double cone $\beta = \omega + \theta$, and then $\beta = \omega - \theta$ for the subsequent converging part, Fig. 2b. Since neither the initial absorption into the diverging part of the double cone nor the subsequent absorption into the converging part is piston-like, the absorption rate must be calculated explicitly.

In previous work (1), we adopted the dynamic absorption equations of Bosanquet (21). He considered the inertial and viscous forces that acted as the fluid entered a cylindrical capillary tube from a large reservoir (supersource). We recognize two approximations implicit in Bosanquet's approach. Firstly, the shape of the meniscus is ignored when calculating the volume of fluid. Secondly, there is no account made of the recirculation regions behind the edges of the meniscus. The modified

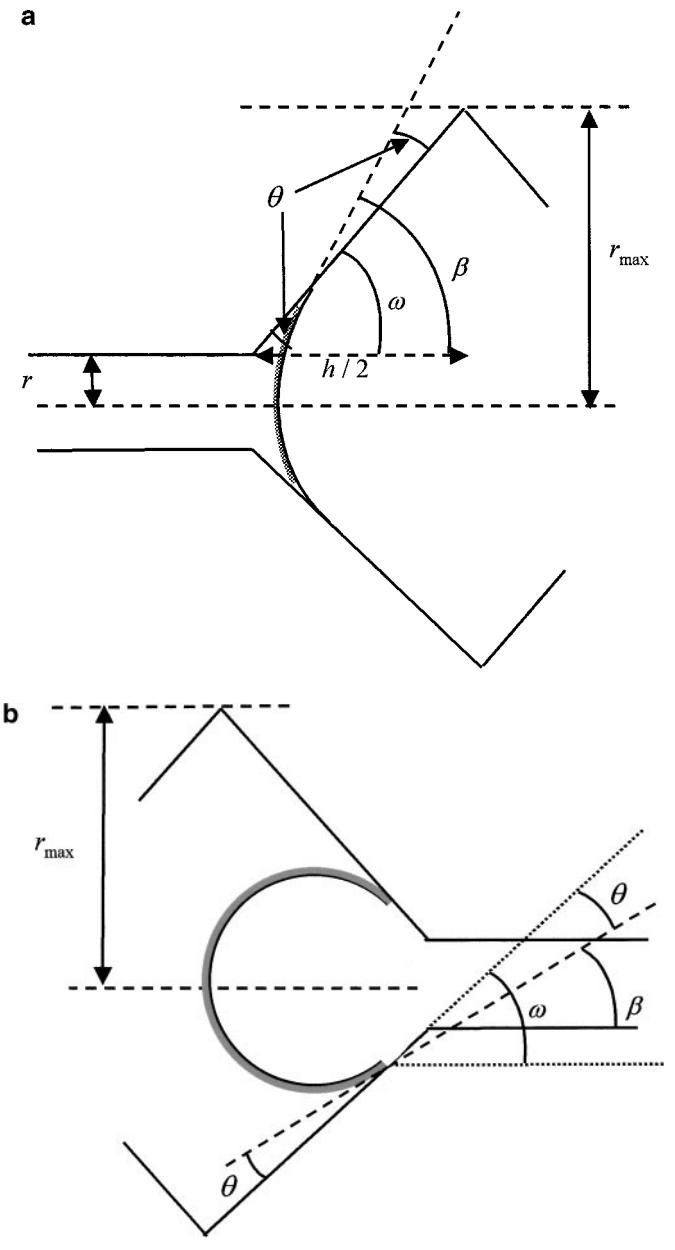

FIG. 2. Geometry of the meniscus of a wetting fluid in (a) the diverging and (b) the converging part of the double cone.

Bosanquet equation of motion is readily shown to be

$$\frac{d}{dt}(xvf(x)) = -axv + bg(x), \quad [5]$$

where

$$a = \frac{8\eta}{\rho r^2}, \quad b = \frac{2\gamma\cos\beta}{\rho r}, \quad \text{and} \quad v = \frac{dx}{dt}, \quad [6]$$

$$f(x) = 1 + \frac{x}{r}\tan\omega + \frac{1}{3}\left(\frac{x}{r}\tan\omega\right)^2, \quad [7]$$

and

$$g(x) = 1 + \frac{x}{r}\tan\omega. \quad [8]$$

Here ρ is the fluid density. The original Bosanquet equation is recovered if we set $\omega = 0$ and $\beta = 0$, which corresponds to $f(x) = g(x) = 1$.

Equation [5] is essentially a second-order differential equation for $\frac{1}{2}x^2$ and does not have a simple analytical solution because of the terms $f(x)$ and $g(x)$. It can be solved numerically, as shown below. As in the original Bosanquet equation, the solution does not have singularities at $x = 0$ but the velocity and acceleration must be nonzero at $x = 0$. These results arise because the Bosanquet model is incorrect near $x = 0$. Improvements have been suggested by Szekely *et al.* (22), who conclude that they are important for times on the order of $(1/a)$. In the present work, we are primarily interested in the total time it takes a fluid to penetrate a conical pore. As shown below, this time is typically much larger than $(1/a)$ and so the Bosanquet model should be adequate.

Equation [5] is first rewritten as a pair of first-order differential equations for the variables $y = \frac{1}{2}x^2$ and $z = xv$ as

$$\frac{dy}{dt} = z \quad [9]$$

$$\frac{d}{dt}(zf(x)) = -az + bg(x). \quad [10]$$

Equation [10] is linear in z and so can be solved numerically using the trapezoidal method provided that an estimate of x at the new time step can be found. Euler's method is applied to [9] for this purpose. The numerical scheme for the solution at time $(n+1)\Delta t$ in terms of the solution at time $n\Delta t$ is then

$$y^{\mathrm{p}}_{n+1} = y_n + z_n\Delta t, \quad x^{\mathrm{p}}_{n+1} = \sqrt{2y^{\mathrm{p}}_{n+1}}, \quad [11]$$

$$z^{\mathrm{c}}_{n+1} = \frac{z_n\left[f(x_n) - a\frac{\Delta t}{2}\right] + \frac{b\Delta t}{2}\left[g(x_n) + g\left(x^{\mathrm{p}}_{n+1}\right)\right]}{f\left(x^{\mathrm{p}}_{n+1}\right) + \frac{a\Delta t}{2}}, \quad [12]$$

$$y^{\mathrm{c}}_{n+1} = y_n + \frac{\Delta t}{2}\left[z_n + z^{\mathrm{c}}_{n+1}\right], \quad x^{\mathrm{c}}_{n+1} = \sqrt{2y^{\mathrm{c}}_{n+1}}, \quad [13]$$

$$v^{\mathrm{c}}_{n+1} = z^{\mathrm{c}}_{n+1}/x^{\mathrm{c}}_{n+1}. \quad [14]$$

Here the superscripts $^{\mathrm{p}}$ and $^{\mathrm{c}}$ denote predicted and corrected values, respectively, and the corrected values are used in the next step. This scheme has the advantage that it is stable for all time steps Δt but, for accurate results, the product $a\Delta t$ should be small compared to unity.

The calculation steps through the diverging part of the conical throat where $\beta = \omega + \theta$, until the throat is half full, and then β changes to $\omega - \theta$ for the converging part. The expression for $f(x)$ also changes to

$$f(x) = 1 + \frac{\tan\omega}{xr}\left(\frac{h^2}{2} - (h-x)^2\right) + \frac{\tan^2\omega}{xr^2}\left(\frac{h^3}{12} - \frac{(h-x)^3}{3}\right)^2, \quad [15]$$

and the expression for $g(x)$ to

$$g(x) = 1 + \frac{(h-x)}{r}\tan\omega. \quad [16]$$

Construction and Wetting of a Three-Dimensional Network

The following procedure was used to generate a Pore-Cor three-dimensional void network. First, the throat skew parameter was used to assign an appropriate number of throat entry radii at each of 100 sizes spaced over a log–linear distribution, for example as shown in Fig. 7 below. Then each throat was allocated a position using a pseudo-random number generator, forming an isotropic structure by ensuring that equivalent numbers of throats were positioned in each Cartesian direction. Then pores of size Cu were added, where $\mathrm{Cu} = \max[r_{\mathrm{i}}]$, and r_{i} are the throats, up to six in number, adjoining the six faces of the cubic pore. Then for each throat,

$$r_{\mathrm{cone}} = \Psi\left(\frac{Q - \min[\mathrm{Cu}_1, \mathrm{Cu}_2]}{4} - r\right) + r, \quad [17]$$

where Cu_1 and Cu_2 are the side lengths of the two pores adjacent to the throat, r is the throat entry radius, and Ψ is the "conicality." Ψ has a maximum value of 1, giving approximately the maximum size of cones that can be fitted into the unit cell without overlapping, and if $\Psi = 0$ the throats are cylindrical.

The wetting equations derived above were used to calculate the wetting flux in each pore and throat in the void network at every time step. It was assumed that inertial flow occurred when fluid began to enter each throat, initially wetting the throat in the form of a monolithic block of fluid (1). As described above, the inertia of the fluid caused a retardation of wetting of the larger pores, at short times after initial entry into a feature, relative to that predicted by the Washburn equation. Once a double-conical throat was completely full, the volumetric flow rate at the throat exit was calculated, and used to calculate the rate of fill of the adjacent pore. A pore could be filled by the fluid from more than one throat, which could start to flow into it at different times. Once a pore was full, it started to fill the throats connected to it that were not already full and that were not already filling from other pores. If at any stage the outflow of a pore exceeded the inflow, then a restriction due to conservation of mass was applied, which removed this imbalance and restricted the flow of fluid further into the network.

The absorption was quantified as F, the fraction of the total void volume that was filled with the fluid at time t. For

comparison with experiment, the absorption was expressed as a Darcy distance $L = 10\ QF$. This corresponded to the volume-averaged distance between the supersource and the wetting front.

MATERIALS AND METHODS

Solid Samples

The sample material was ground calcium carbonate, which is used as a main component in some paper coatings. It was compacted. The grain size before compaction, and the compaction pressure itself, could be carefully controlled to give a reproducible and relatively homogeneous porous structure. Such homogeneity was required so that similar portions of the same specimen could be used for the fluid absorption and mercury porosimetry experiments. The sample was consolidated and therefore did not require containment in a sample vessel during the absorption experiments, thus eliminating uncertainties of interactions between the fluid and such a vessel.

The specific material used in this study was commercially available calcium carbonate (OMYA Inc. Hydrocarb OG), with 60% by weight of the particles less than 2 μm in diameter. This material had been wet ground in the presence of a polyacrylic dispersing agent, and then spray-dried. The powder was compacted in a steel die at 259.4 ± 2.7 MPa as described in Gane *et al.* (23). Part of each sample was studied by mercury porosimetry to determine its percolation characteristics, and the rest used for the absorption experiments. Three samples were used, which we refer to as samples 59, 61, and 66, which had porosities of 23.0, 24.6, and 23.8%, respectively. These porosities were as similar to each other as could be achieved experimentally. So although the separate samples are identified in this work, for purposes of discussion they are considered equivalent.

The static contact angle of each fluid was measured on a surface of marble, which had been wet ground using the same dispersing agent as for the absorption and porosimetry samples. The microroughness of the surface was measured with a confocal laser scanning microscope (Lasertec 1LM21).[2] The microscope scanned perpendicular to the surface at 4780 points with a spacing of 0.38 μm, and measured a surface roughness variance of 0.37 μm^2.

Liquid Samples

The absorbed liquids were a range of alcohols that are components of waterborne inks, namely ethanediol, 1,3-propandiol, butanediol, butanetriol, and 1-octanol (Fluka,[3] research grade). The properties of these fluids are shown in Table 1. Water was used for simulation purposes only, because if used experimentally it can cause the samples to disintegrate. For ease of recognition in the table, the contact angles are shown in degrees, but in the equations their units are radians.

TABLE 1
Properties of Test Liquids at 20°C

Liquid	Surface tension, γ (N m^{-1})	Density, ρ (kg m^{-3})	Viscosity, η (kg m^{-1}s^{-1})	Static contact angle, θ (°)
Water[a]	0.07275	998	0.001	0, 10[b]
Ethanediol	0.048	1113	0.02	21.3
1,3-Propandiol	0.0458	1053	0.0571	34.5
Butanediol	0.0366	1004	0.135	39.7
Butanetriol	0.0559	1185	1.9	30
1-Octanol	0.0275	824	0.01064	20

[a] Only used for simulation purposes.
[b] Contact angles used in simulation.

Mercury Porosimetry

A Micromeritics Autopore III mercury porosimeter[4] was used to measure the percolation characteristics of the samples. The maximum applied pressure of mercury was 414 MPa (60,000 psia), equivalent to a Laplace throat diameter of 0.004 μm, Eq. [1]. Small samples were used, each of around 1.5 g in weight. The equilibration time at each of the increasing applied pressures of mercury was set to 60 s.

The mercury intrusion measurements were corrected for the compression of mercury, expansion of the glass sample chamber or "penetrometer," and compressibility of the solid phase of the sample by use of the following equation from Gane *et al.* (24):

$$V_{\text{int}} = V_{\text{obs}} - \delta V_{\text{blank}} + \left[0.175\left(V^1_{\text{bulk}}\right)\log_{10}\left(1 + \frac{P}{1820}\right)\right] - V^1_{\text{bulk}}(1 - \Phi^1)\left(1 - \exp\left[\frac{(P^1 - P)}{M_{\text{ss}}}\right]\right). \quad [18]$$

V_{int} is the volume of intrusion into the sample, V_{obs} the intruded mercury volume reading, δV_{blank} the change in the blank run volume reading, V^1_{bulk} the sample bulk volume at atmospheric pressure, P the applied pressure, Φ^1 the porosity at atmospheric pressure, P^1 the atmospheric pressure, and M_{ss} the bulk modulus of the solid sample. The volume of mercury intruded at the maximum pressure, once corrected for sample compression effects, was used to calculate the porosity of each sample.

RESULTS AND DISCUSSION

Simulated Wetting in Single Throats

Figure 3 shows the change in velocity of water and 1,3-propandiol with distance through a double-cone geometry, using

[2] Lasertec 1LM21 is a product name of Lasertec Corporation, Unit 4, Wendell Court, 16/20 Wendell Road, London W12 9RT,UK.
[3] Fluka Chemie AG,Industriestrasse 25, CH-9470 Buchs, Switzerland.
[4] Auropore III is a product name of Micromeritics, One Micromeritics Drive, Norcross, GA 30093, USA.

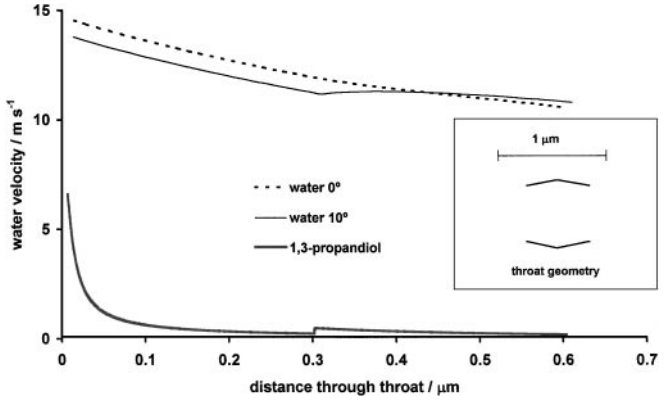

FIG. 3. Change in velocity of water (contact angles 0° and 10°) and 1,3-propandiol with distance through a double-conical throat where r, h, and r_{max} are 0.609, 0.604, and 0.76 μm respectively.

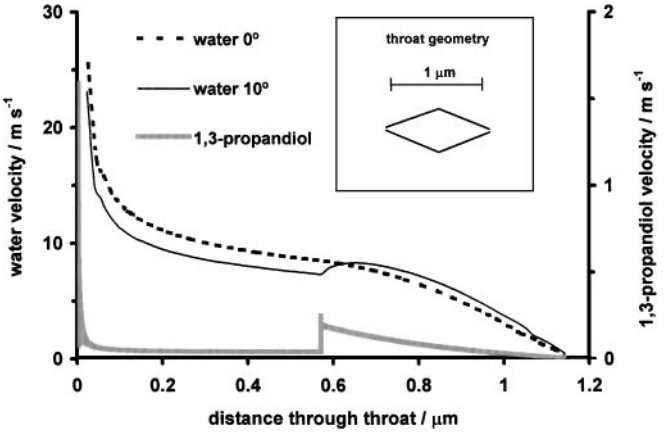

FIG. 4. Velocities of the wetting fronts for the same fluids as in Fig. 3, but flowing through a double cone where r, h, and r_{max} are 0.03, 1.14, and 0.567 μm, respectively. 1,3-Propandiol velocity is shown on the right-hand axis.

a time step of 1 ns corresponding to $a\,\Delta t \approx 2 \times 10^{-2}$. r, h, and r_{max} are 0.609, 0.604, and 0.76 μm, respectively, giving a geometry as shown in the figure. The results for two different contact angles are shown for water, namely 0° and 10°. It can be seen that the velocity of the wetting front of water decreases after the initial entry until it reaches the maximum diameter of the double cone. For the larger contact angle the fluid accelerates before decelerating after the maximum diameter. As expected, the velocity of the water with contact angle 0° is larger than that of water with contact angle 10° in the diverging part, because the former is more wetting and the component of force in the axial direction of the wetting force along the contact line is therefore greater. For the converging part of the throat, the effect of contact angle change is less predictable, and in this case the velocity of the water with contact angle 10° becomes greater than that of the more wetting liquid. The velocity for the 1,3-propandiol decreases much more rapidly than that of the water in the diverging part of the double cone. At the start of the second half of the double cone the velocity undergoes a slight increase and then decreases again slowly through to the exit.

Figure 4 shows the velocities of the wetting fronts for the same fluids but flowing through a double cone, where r, h, and r_{max} are 0.03, 1.14, and 0.567 μm, respectively. The decreasing velocity of water in the diverging part of the double cone is apparent. The velocity increases slightly in the converging part of the double cone for the higher contact angle with water and then decreases again. In these calculations the values of $a\Delta t$ are approximately 9 for water and 48 for 1,3-propandiol. These values are clearly not small compared with unity and so the accuracy of the solution is questionable. In the case of 1,3-propandiol (right-hand axis) the solution exhibits its inaccuracy in the form of oscillations. These have been exaggerated in Fig. 5 by use of logarithmic axes. When the calculations are repeated with a time step of 10^{-3} ns, corresponding to $a\,\Delta t \approx 5 \times 10^{-2}$, a much smoother solution is obtained, as shown. However, the oscillations occur over a very small portion of the total throat length (~2.5%) and decay to the accurate solution over the remainder—to the right of the oscillations the two curves lie on top of each other. It is also found that the total time taken for fluid to traverse the throat is insensitive to the time step used. Therefore it is argued that a time step of 1 ns is acceptable as a compromise between the accuracy of solution and reasonable overall computing times. For single throats, it is possible to backtrack and reduce the time step when inaccuracies occur. However, the calculation in this work is carried out over some 4000 different features, at different degrees of filling, and individual backtracks would therefore slow the calculation down to an unacceptable degree.

Generation of a Simulated Void Structure

The experimental intrusion curves provided the percolation characteristics necessary for the generation of the void structure using Pore-Cor. Figure 6 shows the fully corrected mercury intrusion curve for sample 61 and also the fit of a Pore-Cor structure containing cylindrical throats. The applied mercury pressures have been converted to diameters by application of

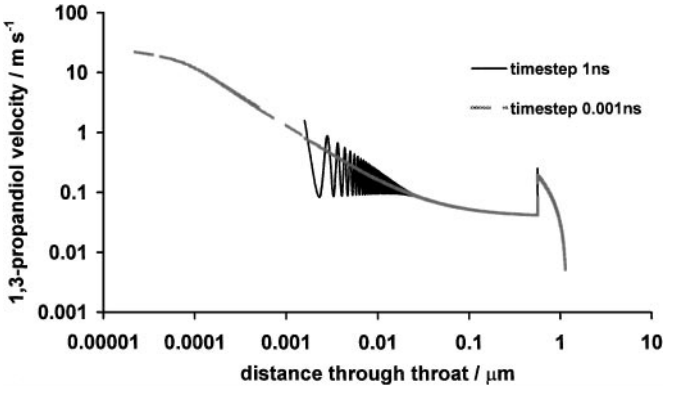

FIG. 5. 1,3-Propandiol velocity as described in the legend to Fig. 4, but with logarithmic axes.

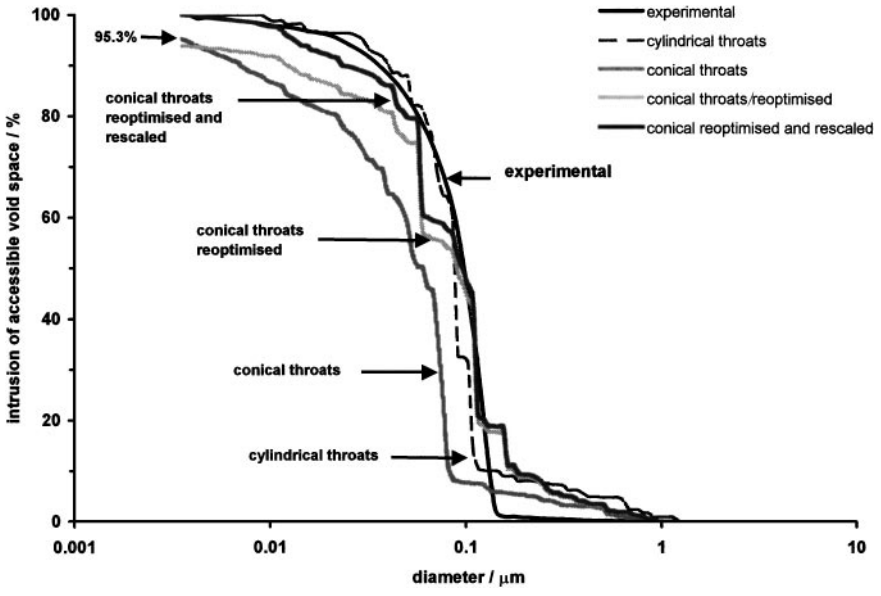

FIG. 6. Fully corrected experimental mercury intrusion curve for sample 61, and simulated curves.

the Laplace equation [1], and the intrusion scaled from 0 to 100% of the experimentally accessible intrusion volume. One-hundred percent on this axis corresponds to complete filling up to the experimentally measured porosity of 24.6%.

If the throats in the same simulated structure were made maximally conical ($\Psi = 1$), then the hold-up effects reduced the simulated intrusion of the mercury, as shown in Fig. 6. It can be seen that at the maximum applied mercury pressure, or minimum intruded Laplace diameter, a maximum intrusion of only 95.3% of the simulated void space was now achievable, corresponding to an intruded porosity of $0.953 \times 24.6\% = 23.4\%$. Also, the simulated intrusion curve has moved toward smaller pore and throat sizes, due to the effects described in the discussion of Eq. [4]. If this new structure was reoptimized to fit the experimental curve (in this case by reducing the connectivity and increasing the relative number of large throats), a better fit resulted but the maximum intrusion reduced to 93.9%, or an intruded porosity of 23.1%. To correct this, the total porosity of the simulated structure had to be increased to 26.2%, so that the intruded porosity then matched the experimental porosity of 24.6%. This last step made a minimal difference to the simulated absorption characteristics of a wetting fluid, for all the samples investigated. The Pore-Cor fitting parameters are summarized in Table 2. Pore-Cor fits the entire intrusion curve, but in the literature the intrusion curve is often characterized by a single point, namely the characteristic throat diameter d_{50}, which is the throat-entry size at which 50% of the experimentally intrudable void space has been intruded. For sample 61, the simulated d_{50} was 0.090 μm compared to an experimental value of 0.098 μm, as shown in both Fig. 6 and Table 2.

The corresponding size distributions of pores and throats for the cylindrical Pore-Cor structure and for the conical throat structure for sample 61 are shown in Fig. 7. It was necessary to use a pore skew of 1.4 with the cylindrical throats to match the experimental porosity. This pore skew generated a sharp peak in the distribution, comprising 19.4% of the total number of pores at the maximum size of 1.218 μm. We consider the use of pore skew to bulk up the pores, and generate the correct porosity, to be less satisfactory than the use of conical throats. Both methods are arbitrary to an extent, but the peak produced

TABLE 2
Summary of Experimental and Simulated Characteristics

Sample	Sim throat type	Sim pore skew	Sim throat skew	Sim connectivity	Exp porosity (%)	Sim porosity with hold-up (%)	Total sim porosity without hold-up (%)	Exp characteristic throat diameter, d_{50} (μm)	Sim characteristic throat diameter, d_{50} (μm)
59	Conical	1	0.09	2.9	23.0	23.0	24.4	0.091	0.111
61	Conical	1	0.12	2.6	24.6	24.6	26.2	0.098	0.090
66	Conical	1	0.13	2.6	23.8	23.8	25.4	0.091	0.090
66	Cylindrical	1.2	1.15	3.4	23.8	No hold-up	23.8	0.091	0.070

Note. Exp = experimental, sim = simulated. Hold-up is defined as the additional pressure that is necessary to apply to a fluid for it to enter the diverging part of a double cone, relative to the pressure required for entry into a cylinder with the same size of entry.

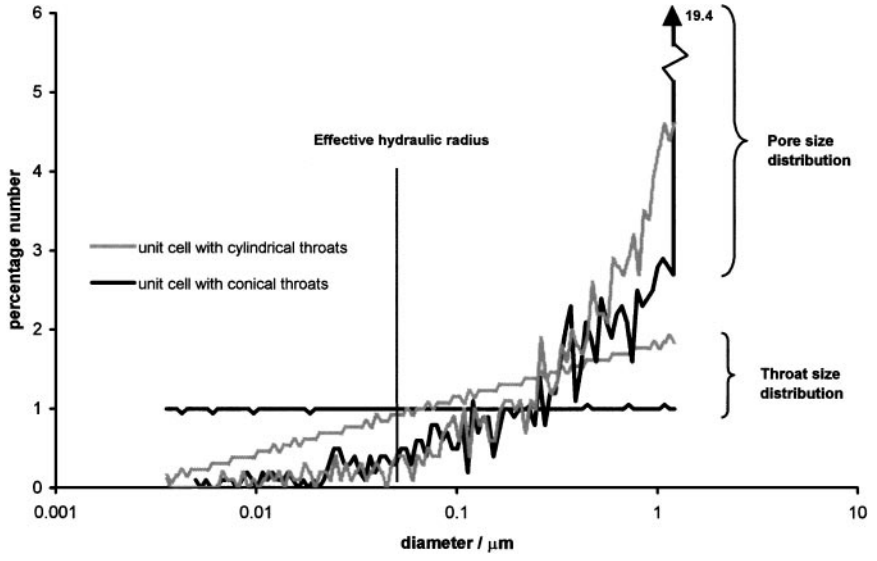

FIG. 7. Size distributions of pores and throats for the cylindrical Pore-Cor structure and the conical throat structure for sample 61.

by the pore skew parameter cannot be confirmed, for example, using image analysis of micrographs of the real void structure. The use of conical throats increases the porosity up to the experimental value in a more structurally realistic manner without causing the sharp peak in the size distribution. A secondary effect is that when conical throats are introduced, the sizes of the adjoining pores must be increased to maintain a match with the experimental percolation characteristics, Eq. [4], which also increases the simulated porosity in the desired way.

Table 2 summarizes the optimum Pore-Cor parameters for all three samples 59, 61, and 66. The simulated structure of the void space of sample 59, incorporating conical throats, is shown in Fig. 8.

Sensitivity Analysis

The "inversion" of a mercury intrusion curve by Pore-Cor gives a simulated void structure with the same percolation characteristics as the experimental sample. However, the solution is not unique—there are an infinite number of void structures that could give rise to the same intrusion curve. This problem is circumvented by applying arbitrary restrictions to the geometry of the simulated void structure. An extreme example of this is the effective hydraulic radius approximation, in which the geometry is so restricted that there is only a single solution to the percolation curve, characterized by a single radius R, Eq. [2]. The geometry of the Pore-Cor voids structure is also restricted—to a unit cell of 1000 pores and up to 3000 double-conical throats. However, this restriction is much less than for the EHR approximation, and consequently many different Pore-Cor unit cells could give the correct percolation curve. Thus the Pore-Cor parameters shown in Table 2 are to some extent arbitrary. This arbitrariness is probed in the current version of the software by creating different "stochastic generations" of structures generated by different sets of random numbers. Although the different stochastic generations give rise to unit cells that look slightly different from each other, the unit cells have the same wetting characteristics to within the bounds of the trends that will be discussed here. Evidence of this was given in an earlier publication for the wetting of porous calcium carbonate blocks (1), and a full sensitivity analysis has recently been carried out for a model of soil (17). Current work on the Pore-Cor model involves the optimization of the structure using a Boltzmann-annealed Simplex, which will find an optimum structure within the multi-dimensional fitting-parameter space, and carry out a full sensitivity analysis by probing the parameter space adjacent to the optimum point.

Wetting of the Simulated Void Structure

Figure 9 shows the fractional wetting F of sample 61 against time for 1,3-propandiol. The time step was 1 ns, for the reasons discussed previously, and each of the calculations typically took 20 h on a 600-MHz personal computer. The graph shows the increased rate of absorption as the throats are changed from cylindrical ($\Psi = 0$) to the conical limit ($\Psi = 1$). The distribution of cone angles ω corresponding to $\Psi = 1$ for this structure is shown as a histogram in Fig. 10.

The simulated absorption of the range of alcohols is shown in Fig. 11.

Wetting of the Experimental Samples

The rate of liquid uptake was measured gravimetrically using an automated PC-linked Mettler Toledo AT460[5] microbalance

[5] Toledo AT460 is a product name of Mettler-Toledo AG, CH-8606 Greifensee, Switzerland.

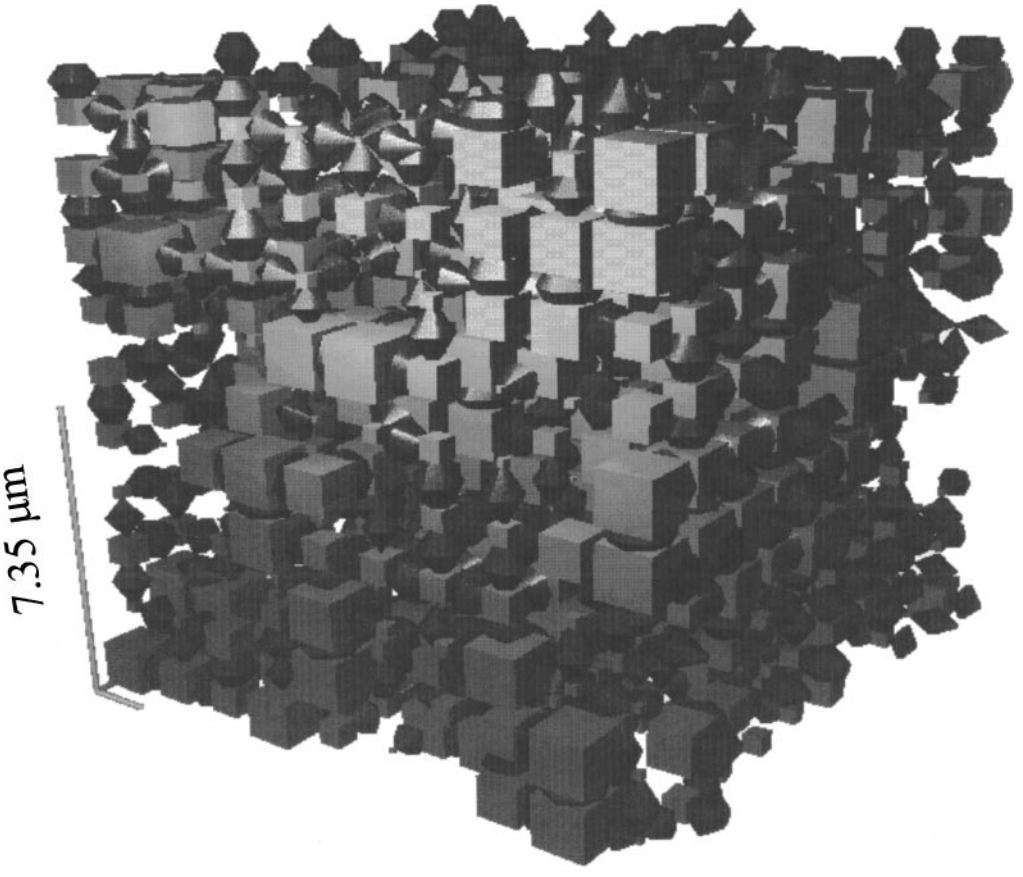

FIG. 8. Double-conical throat structure for sample 61.

with a precision of 0.1 mg, capable of 2.7 measurements per second, under a stream of nitrogen flowing at 1 liter per minute.

The experiments in this study were performed on samples equilibrated for more than 48 h at 23.0 ± 1.5°C under nitrogen. Details of the method and the apparatus are given in Schoelkopf *et al.* (1).

The results are shown in Fig. 12. The experimental absorption has been corrected for the "wetting force" jump of the liquid up

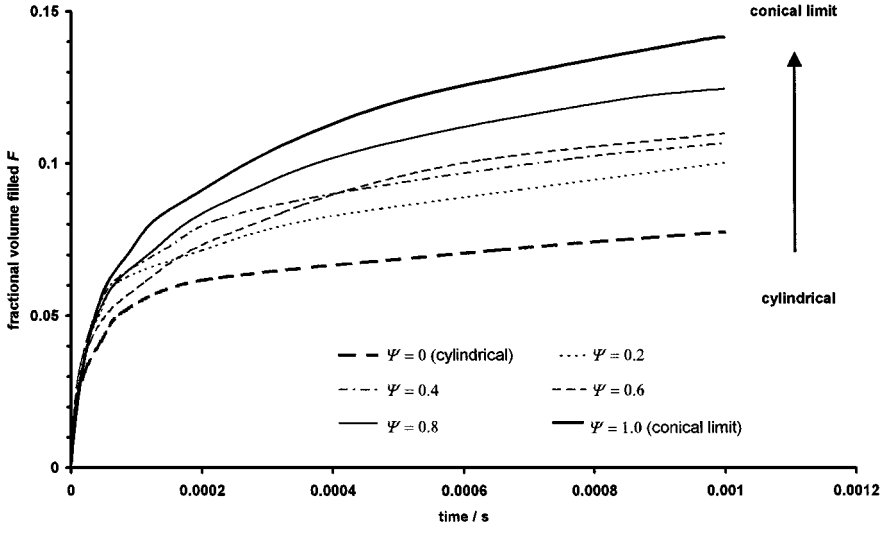

FIG. 9. Fractional wetting F of sample 61 against time for 1,3-propandiol.

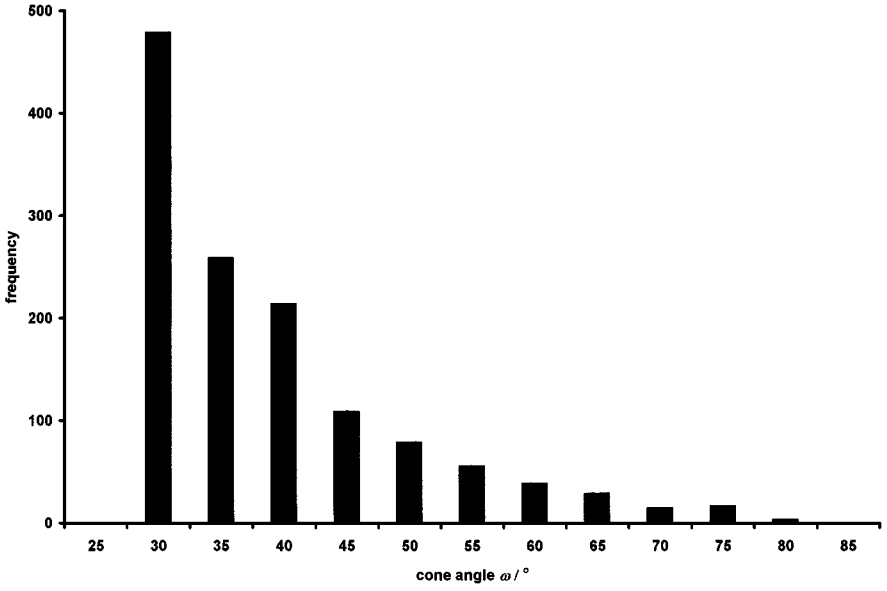

FIG. 10. The distribution of cone angle ω corresponding to conicality $\Psi = 1$ for the structure shown in Figure 8.

onto the bottom surface of the sample (1). The Appendix details the equations used for this correction, which involves an extrapolation of the apparent weight curve to time zero while ignoring the first few experimental points involved in the wetting jump. Although this extrapolation corrected for oscillations caused by the inertia of the meniscus as it jumped, there remained uncertainties in the exact start time of the experiment, estimated at ± 0.2 s, because of these effects. The experimental points up to 1 s were therefore considered to be of low accuracy. Such an uncertainty is considered a major cause of the difference between the experimental absorption curves for propandiol in samples 61 and 66. The uncertainties are shown as horizontal error bars for these samples in Fig. 12.

Comparison between Simulation and Experiment

The experimental measurements are over a timescale much longer than that of the simulated measurements, and do not overlap the simulated values with respect to time. They also have

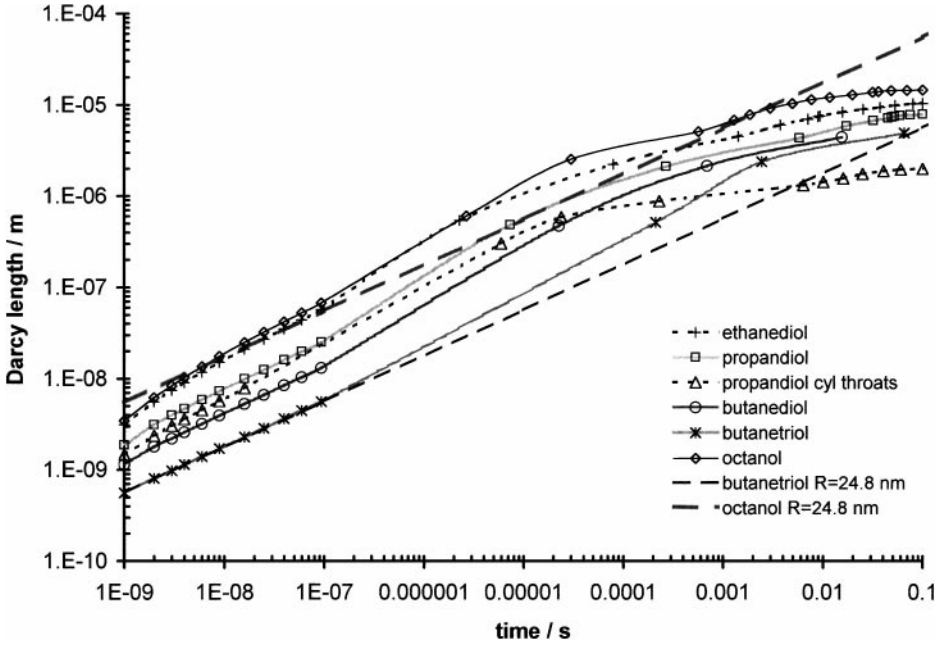

FIG. 11. Simulated absorption of the range of alcohols.

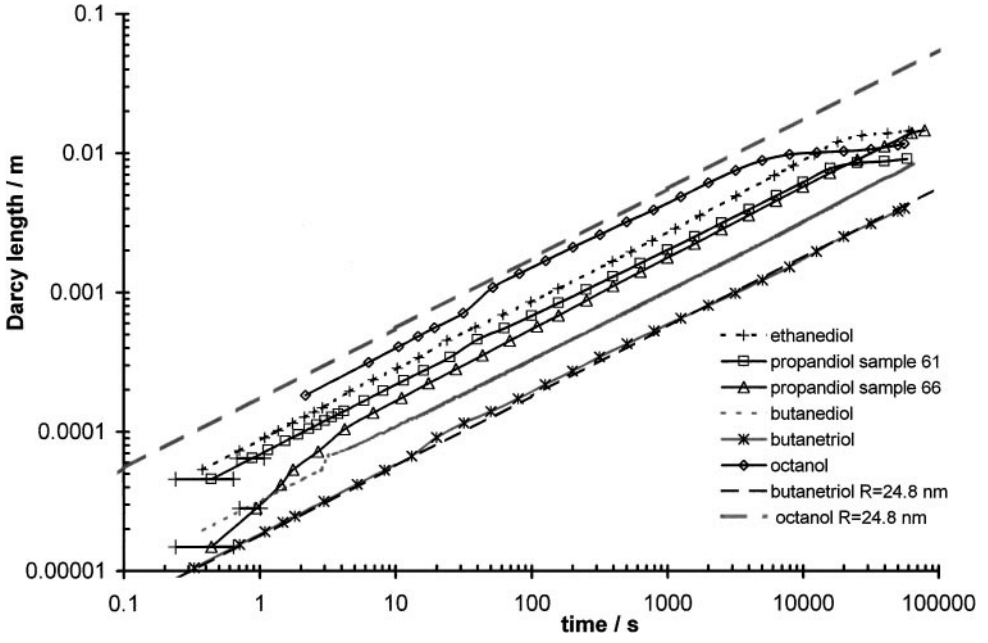

FIG. 12. Experimental absorption curves.

different boundary conditions (1). However, it can be seen that the initial rates of the simulated absorption exhibit a correspondence with the overall rates of the experimental absorption. The trends with different fluids are also similar between simulation and experiment. Figures 11 and 12 also show the previously published simulated and experimental absorption curves (Δ) for 1,3-propandiol in sample 66 (1). This previous Pore-Cor simulation used cylindrical rather than double-conical throats. It can be seen that there is a discrepancy between the simulated and experimental values in this case greater than that for the current simulations. The discrepancy is clearer in Fig. 13, discussed below.

Figures 11 and 12 also show the absorption of octanol and butanetriol predicted by the effective hydraulic radius approximation, Eq. [2]. An effective hydraulic radius R of 24.8 nm gives curves closest to those observed. Figure 7 shows that the corresponding diameter of 49.6 nm lies just below the geometric mean of diameter 65.9 nm of the size distributions of the simulated voids.

The EHR curves are plotted as a horizontal straight line of value 1 in Fig. 13, and the simulated and experimental absorption of octanol and butanetriol are plotted relative to this value. The data are the same as in Figs 11 and 12, just presented

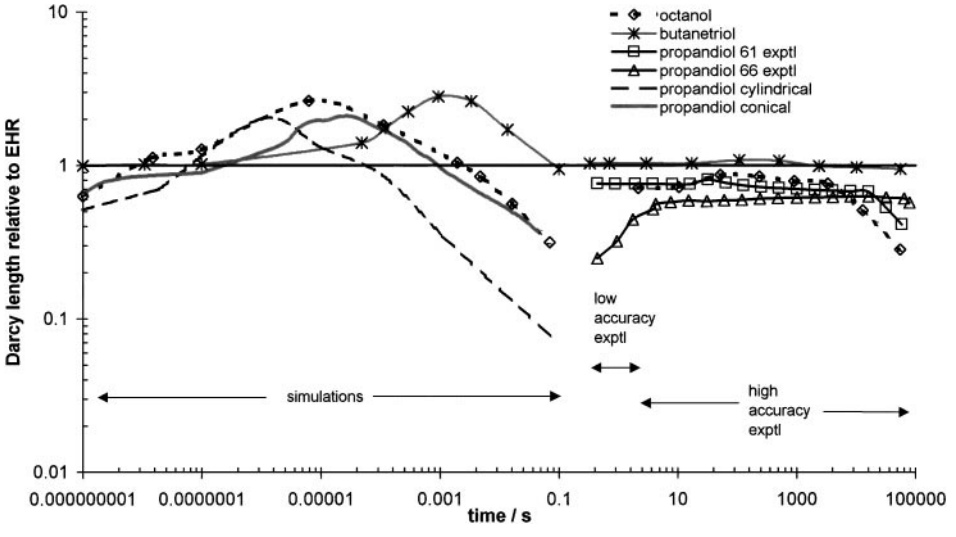

FIG. 13. Absorption relative to the EHR approximation for octanol and butanetriol with $R = 24.8$ nm.

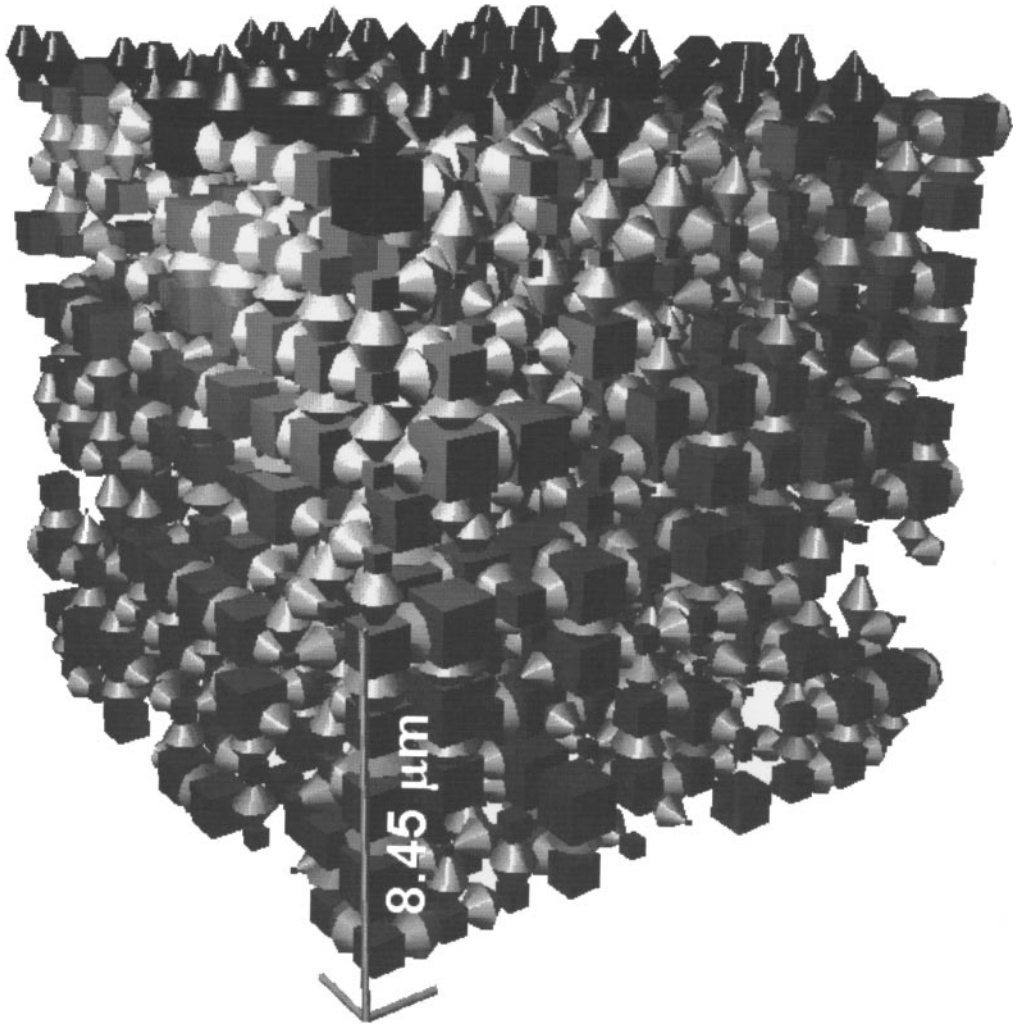

FIG. 14. Absorption of butanetriol, shown dark, from the top face of the unit cell for sample 59 at $t = 200$ μs.

differently. It can be seen in Fig. 13 that the absorption of butanetriol is nearly twice that expected from the EHR approximation at around 1 ms. The 1-octanol absorption varies between 0.6 and 1.9 times that of the EHR absorption. Figures 14 and 15 show the absorption of butanetriol (shown dark) for sample 59 for both 200 μs and 8 ms—either side of the maximum in the absorption rate. It can be seen from the diagrams that the intrusion begins to slow down when lateral movement of fluid is reduced. At 200 μs, the fluid has entered most of the top surface conical throats, and one or two pores connected to them, Fig. 14. At 8 ms, the possibilities of lateral movement at the top of the unit cell have been exhausted, and lateral movement from one unit cell to its identical neighbors is also prevented, because the neighbors are also identically full, Fig. 15. The regions over which the simulated curves begin to show reduced absorption in Fig. 11, emphasized in Fig. 13, mark the times at which the periodic boundary condition begins to affect the absorption. As discussed in a previous work (1), this condition is artificially severe because of the small size of the unit cell, and causes the tail-off of the simulated absorption relative to the experimentally observed absorption.

The experimental curves shown in Figs. 12 and 13 show that butanetriol follows an EHR type of absorption, whereas 1-octanol absorbs considerably less than expected at times greater than 1000 s. The difference in behavior arises from the difference in properties of butanetriol and octanol, the former being 180 times more viscous and 43% denser (Table 1).

Comparing the experimental and simulated results for each alcohol shown in Fig. 13, we conclude firstly that experimental measurements of butanetriol absorption suggest EHR absorption, whereas the simulation shows absorption around 1 ms much greater than would be inferred from this experimental EHR behavior. Secondly, the simulated absorption of the less viscous and less dense 1-octanol shows positive deviations from EHR at times much shorter than those of butanetriol, which again could not be inferred from the experimental results, which show initial EHR behavior followed by a reduction relative to EHR.

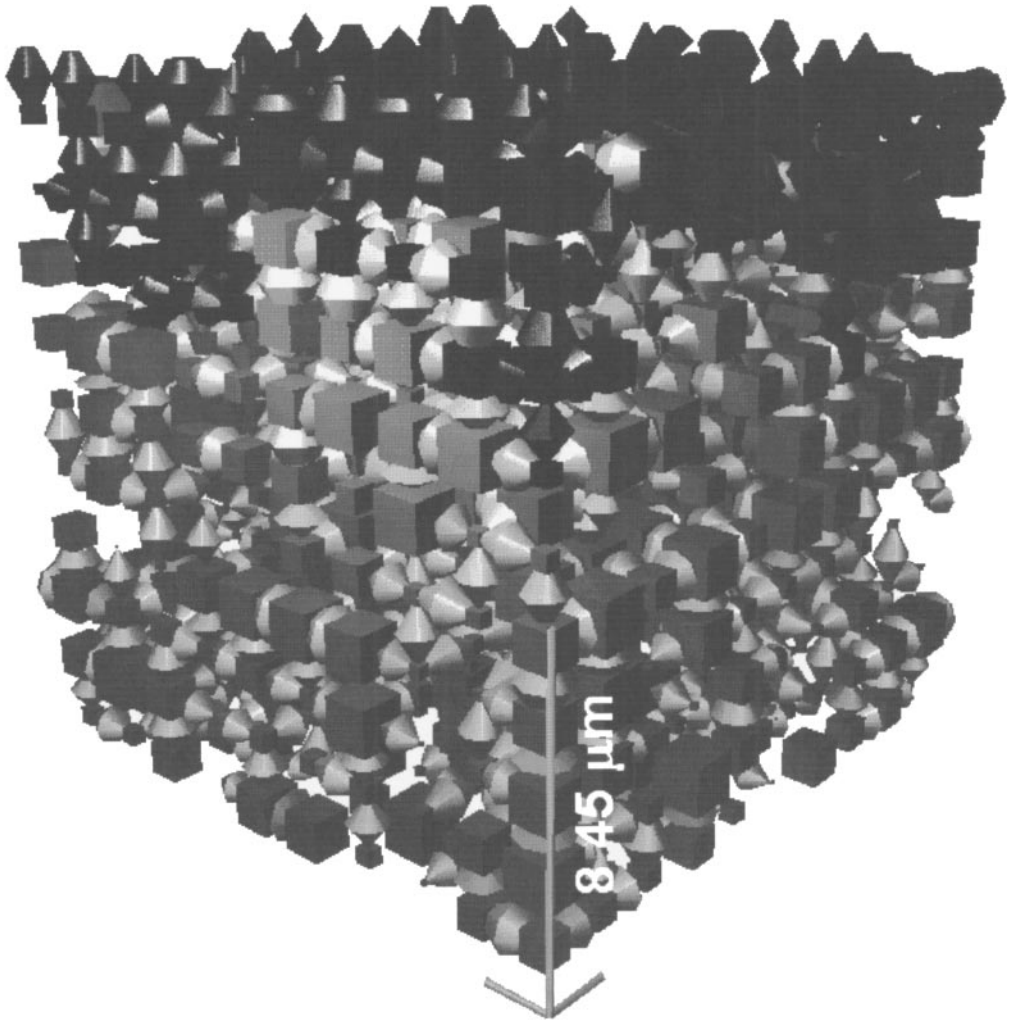

FIG. 15. The same as described in the legend to Fig. 14, but at 8 ms.

What must also be remembered is that the Darcy lengths shown in Figs. 11–13 are volume-averaged positions of the wetting front. These averages mask the development of preferential pathways through the void structure, which lead to highly heterogeneous wetting fronts, as exemplified by Fig. 15. They also mask the inertial effects that occur in each feature, and that make the wetting of larger features by denser liquids slower than expected. Overall, the fluids will wet via preferential pathways, which are well connected throughout the structure, and which follow tracks containing features smaller than would be predicted by a Washburn approach that ignores inertia.

SUMMARY

The geometry of the Pore-Cor unit cell structure has been modified to represent more realistic void shapes within a porous material, in this case compacted calcium carbonate powder. The shapes of the throats have been changed from cylindrical tubes to a double-conical shape incorporating a diverging and then converging geometry. In effecting this change one is clearly replacing one arbitrary parameter (pore skew) with another (conicality). However, the resulting structure assigns additional porosity in a manner that more closely resembles the structures of natural samples. It also incorporates an additional degree of heterogeneity within the sample, which again is a step closer to reality. This heterogeneity is in the form of geometric variations, which cause hold-up of nonwetting fluids and differential acceleration of wetting fluids. Such effects could also be caused by different surface interaction energies, and the increased heterogeneity in the geometry can also be regarded as a representation of the heterogeneity of surface interactions within a real sample.

The effect of the change in throat shape has been shown for both wetting and nonwetting fluids. The structure of the unit cell was optimized so that its intruded porosity was identical with

the experimental sample, and so that the simulated nonwetting fluid (mercury) intrusion curve matched the experimental curve as closely as possible. Absorptions into this structure showed deviations from the EHR approximation. The absorption rates of five alcohols were measured and the simulated absorption curves were then compared to these. The beginnings of the simulation curves have similar gradients to the experimental curves and track in the same order for increasing viscosity. Plotting the results relative to the EHR approximation highlights the trends, and shows how the advancement of the wetting front, expressed as a Darcy length, differs very significantly from that which would occur in a single tube or bundle of tubes. Overall, the fluids will wet via preferential pathways, which follow well-connected tracks containing features smaller than would be predicted by a Washburn approach that ignores inertia. These effects show up on the very short timescales of the simulation, and are of great importance in industrial processes such as printing that involve fast absorption.

APPENDIX

Smoothing equations for the apparent weight change with time during the absorption of different fluids, where m is the apparent weight (g), t the time (s), and R^2 is the standard measure of goodness of fit, unrelated to the effective hydraulic radius R. Equation types are the simplest in each case with $R^2 > 0.997$.

Ethanediol

$$m = (a + ct^{0.5} + et + gt^{1.5})/(1 + bt^{0.5} + dt + ft^{1.5})$$

$$a = 4.3561153, \quad b = -0.009256348, \quad c = -0.043688281,$$

$$d = 1.7126548e - 5, \quad e = 0.000110932669,$$

$$f = 8.6388785 \times 10^{-8}, \quad g = 2.5185248 \times 10^{-7},$$

$$R^2 = 0.9997$$

1,3-Propandiol

$$m = (a + ct^{0.5} + et)/(1 + bt^{0.5} + dt + ft^{1.5})$$

$$a = 2.0413123, \quad b = -0.008960098, \quad c = -0.020493998,$$

$$d = 2.2832422 \times 10^{-5}, \quad e = 6.6193272 \times 10^{-5},$$

$$f = 2.7494107 \times 10^{-8}, \quad R^2 = 0.9994$$

Butanediol

$$m^2 = a + bt^{0.5}$$

$$a = 54.483527, \quad b = -0.018292355, \quad R^2 = 0.9992$$

Butanetriol

$$m^{-1} = a + bt^{0.5}$$

$$a = 0.49226177, \quad b = 0.00016415427, \quad R^2 = 0.9988$$

1-Octanol

$$m = (a + ct^{0.5} + et)/(1 + bt^{0.5} + dt + ft^{1.5})$$

$$a = 23.01395, \quad b = -0.0095973436, \quad c = -0.22418864,$$

$$d = 0.00012091329, \quad e = 0.0027948089,$$

$$f = 5.3889712 \times 10^{-9}, \quad R^2 = 0.9978$$

ACKNOWLEDGMENT

We are grateful to Joseph Matthews, of Corpus Christi College, University of Oxford, for programming the Pore-Cor algorithm, which draws the conical throats.

REFERENCES

1. Schoelkopf, J., Ridgway, C. J., Gane, P. A. C., Matthews, G. P., and Spielmann, D. C., *J.Colloid Interface Sci.* **227,** 119 (2000).
2. Wardlaw, N. C., Li, Y., and Forbes, D., *Trans. Por. Med.* **2,** 597 (1987).
3. Baldwin, C. A., Sederman, A. J., Mantle, M. D., Alexander, P., and Gladden, L. F., *J.Colloid Interface Sci.* **181,** 79 (1996).
4. Tsakiroglou, C. D., and Payatakes, A. C., *J.Colloid Interface Sci.* **137,** 315 (1990).
5. Borhan, A., and Rungta, K. K., *J.Colloid Interface Sci.* **155,** 438 (1993).
6. Ransohoff, T. C., and Radke, C. J., *J. Colloid Interface Sci.* **121,** 392 (1988).
7. Tang, L.-H., and Tang, Y., *J. Phys. II* **4,** 881 (1994).
8. Dong, M., and Chatzis, I., *J. Colloid Interface Sci.* **172,** 278 (1995).
9. Ma, S. X., Mason, G., and Morrow, N. R., *Colloids Sur. A-Physicochem. Eng. Asp.* **117,** 273 (1996).
10. Yost, F. G., Rye, R. R., and Mann, J. A., *Acta mater* **45,** 5337 (1997).
11. Weislogel, M. M., and Lichter, S., *J. Fluid. Mech.* **373,** 349 (1998).
12. Maisch, E., Renzow, D., Sell, P.-J., and Walitza, E., *Z. Flugwissenschaften Weltraumforschung* **5,** 189 (1981).
13. Gavrilenko, P., and Gueguen, Y., *Tectonophysics* **217,** 91 (1993).
14. Matthews, G. P., Ridgway, C. J., and Small, J. S., *Mar. Pet. Geo.* **13,** 581 (1996).
15. Lee, L.-H., *J. Adhes. Sci. Technol.* **7,** 583 (1993).
16. Ridgway, C. J., Ridgway, K., and Matthews, G. P., *J. Pharm. Pharmacol.* **49,** 377 (1997).
17. Peat, D. M. W., Matthews, G. P., Worsfold, P. J., and Jarvis, S. C., *Europ. J. Soil. Sci.* **51,** 65 (2000).
18. Matthews, G. P., Ridgway, C. J., and Spearing, M. C., *J. Colloid Interface Sci.* **171,** 8 (1995).
19. Washburn, E. W., *Phys. Rev.* **17,** 273 (1921).
20. Lucas, R., *Kolloid Z.* **23,** 15 (1918).
21. Bosanquet, C. H., *Phil. Mag. Ser. 6* **45,** 525 (1923).
22. Szekely, J., Neumann, A. W., and Chuang, Y. K., *J. Colloid Interface Sci.* **35,** 273 (1971).
23. Gane, P. A. C., Schoelkopf, J., Spielmann, D. C., Matthews, G. P., and Ridgway, C. J., *Tappi J.* **83,** 77 (2000).
24. Gane, P. A. C., Kettle, J. P., Matthews, G. P., and Ridgway, C. J., *Ind. Eng. Chem. Res.* **35,** 1753 (1995).